



# Multi-slice computed tomography radiomics combined with serum alpha-L-fucosidase: a potential biomarker for precise identification of pleomorphic adenoma and Warthin tumor

Qinghan Yan<sup>1#</sup>, Lingzi Liao<sup>2#</sup>, Xin Wang<sup>2</sup>, Xianlin Zeng<sup>2</sup>, Leyang Zhang<sup>2</sup>, Dengqi He<sup>3</sup>

<sup>1</sup>The First School of Clinical Medicine, Lanzhou University, Lanzhou, China; <sup>2</sup>Department (Hospital) of Stomatology, Lanzhou University, Lanzhou, China; <sup>3</sup>Department of Stomatology, The First Hospital of Lanzhou University, Lanzhou, China

**Contributions:** (I) Conception and design: Q Yan, L Liao, L Zhang, D He; (II) Administrative support: D He; (III) Provision of study materials or patients: Q Yan, X Wang; (IV) Collection and assembly of data: Q Yan, L Zhang; (V) Data analysis and interpretation: Q Yan, X Zeng; (VI) Manuscript writing: All authors; (VII) Final approval of manuscript: All authors.

<sup>#</sup>These authors contributed equally to this work.

**Correspondence to:** Dengqi He, MD. Department of Stomatology, The First Hospital of Lanzhou University, 1 Donggang West Road, Lanzhou 730000, China. Email: hedengqi1975@163.com.

**Background:** The rising incidence of parotid gland tumors, with a focus on pleomorphic adenomas (PMA) and Warthin tumors (WT), necessitates accurate preoperative distinction due to their treatment variability and PMA's malignant potential. Traditional imaging, while valuable, has limited accuracy. This study employs multi-slice computed tomography (MSCT) radiomics coupled with serum alpha-L-fucosidase (AFU) levels to develop a diagnostic model aimed at elevating clinical discernment and precision therapy delivery.

**Methods:** Ninety-one patients were randomly assigned to one of two cohorts: training or validation, at a ratio of 7:3 (64 *vs.* 27). The region of interest (ROI) on each tumor from the collected MSCT images was delineated to extract radiomics features. In the training cohort, the least absolute shrinkage and selection operator (LASSO) regression and 5-fold cross-validation were adopted to screen the extracted features and calculate Rad-score. Four diagnostic models were developed after univariate and multivariate logistic regression analysis of Rad-score and clinical factors. The performance of four models was then evaluated in the validation cohort by the comparison of receiver operating characteristic (ROC) curve and calibration curve to select the best one. Finally, the clinical application value of the best model was assessed via the nomogram and decision curve analysis (DCA) curve.

**Results:** Multivariate logistic regression analysis revealed serum AFU, Rad-score and gender as independent diagnostic factors for PMA and WT distinguishment. The nomogram combining the three factors had an area under the curve (AUC) of 0.934 [95% confidence interval (CI): 0.863–1.000] and 0.987 (95% CI: 0.956–1.000) in the training and validation cohorts, respectively, with great goodness-of-fit and clinical value.

**Conclusions:** The optimized nomogram combining MSCT radiomics and AFU improved the accuracy of distinguishing PMA from WT, suggesting its potential for developing new biomarkers.

**Keywords:** Pleomorphic adenoma (PMA); Warthin tumor (WT); radiomics; nomograms; alpha-L-fucosidase (AFU)

Submitted May 28, 2024. Accepted for publication Nov 10, 2024. Published online Dec 27, 2024.

doi: 10.21037/tcr-24-871

**View this article at:** <https://dx.doi.org/10.21037/tcr-24-871>

## Introduction

The incidence rate of salivary gland tumors is increasing every year, most of which occur in parotid glands. The vast majority of parotid gland tumors are pleomorphic adenoma (PMA) and Warthin tumor (WT) (1). The currently applied standard of treatment for PMA is superficial parotidectomy or partial superficial parotidectomy, while WT is treated with extracapsular dissection (2). Extracapsular dissection is not appropriate for PMA because it increases the likelihood of postoperative recurrence. Therefore, it is of great significance to clearly distinguish PMA from WT before surgery.

Radiological examination plays a pivotal role in the preoperative diagnosis of parotid gland tumors (3,4). Multi-slice computed tomography (MSCT) is being increasingly used in the clinical setting due to its advantages of low cost, shorter operation time, and the ability to clearly visualize the location of tumor in relation to surrounding soft and hard tissues, as well as important blood vessels (5).

Physicians ordinarily make a qualitative diagnosis of parotid tumors on radiological images through visual analysis. Such subjective assessment is prone to misdiagnosis. In recent years, radiomics has recently gained interest as a research subject due to the innovation in medical imaging diagnostics brought about by advances in computer technology. Based on artificial intelligence, radiomics can automatically extract repeatable image features that far exceed those obtained by physicians' visual analysis and transform them into high-dimensional data to evaluate, which effectively compensates for the shortcoming of traditional diagnosis depending solely on visual analysis of radiological images (6). Radiomics was first presented in 2012 by the Dutch scholar Lambin, who considered that the spatiotemporal heterogeneous of solid tumors can be exhibited by modern medical imaging, i.e., high-resolution imaging devices can capture both intra-tumoral features and instant pathophysiological information in a non-invasive way, and thus he defined radiomics as the process of high-throughput extraction of image features from radiographic images (7). Radiomics belongs to a typical medical-industrial interdisciplinary field, with five essential steps: image acquisition, image segmentation, feature extraction, feature screening, and model development. In recent years, radiomics have been demonstrated for the diagnosis of many types of cancer, including lung cancer and liver cancer (8). In oral diseases, radiomics can be used for diagnosis of jaw cysts, prognosis analysis of head and neck cancer, and prediction analysis of dry mouth symptoms after radiotherapy. Furthermore, several studies have shown that radiomics can be utilized for preoperative diagnosis of parotid tumors. However, there remains a research gap in identifying parotid tumors using a combination of radiomics and biochemical markers.

Alpha-L-fucosidase (AFU), a lysosomal acid hydrolase found in abundance in liver and kidney tissue cells, is mainly engaged in the catabolism of macromolecular substances such as various glycolipids of fucose and glycoprotein (9). Since Deugnier discovered that serum AFU levels were higher in patients with primary liver cancer in 1980 (10), the relationship between serum AFU and tumor has been extensively researched. Serum AFU level was lower in a range of cancer patients, including ovarian cancer and colorectal cancer, and low serum AFU expression was generally associated with high malignancy grade and poor prognosis (11,12). However, a study by Shah *et al.* showed that serum AFU activity was positively correlated with the severity of oral cancer (13). PMA is a benign tumor that

### Highlight box

#### Key findings

- This study developed a multi-slice computed tomography (MSCT) radiomics model combined with serum alpha-L-fucosidase (AFU) levels to improve the diagnostic accuracy for distinguishing pleomorphic adenoma (PMA) from Warthin tumor (WT) in the parotid gland. The optimized model, integrating AFU, gender, and Rad-score, demonstrated excellent discrimination capability with an area under the curve of 0.987 in the validation cohort and good clinical applicability.

#### What is known and what is new?

- PMA and WT are the most common benign parotid tumors, requiring different surgical approaches. Traditional imaging methods rely on qualitative assessments, which may cause misdiagnosis and inappropriate treatment.
- This study introduces a novel diagnostic model combining MSCT radiomics features and serum AFU levels to provide a quantitative and reproducible approach for differentiating PMA from WT. It also highlights the potential use of AFU as a preoperative biomarker.

#### What is the implication, and what should change now?

- The integration of MSCT radiomics and AFU levels offers a reliable tool for precise preoperative diagnosis of parotid tumors. This approach can improve clinical decision-making by tailoring surgical strategies to specific tumor types and reducing postoperative risks. Future studies should focus on validating this model across larger, multi-center cohorts to confirm its generalizability and explore its role in predicting malignancy risk in PMA patients.

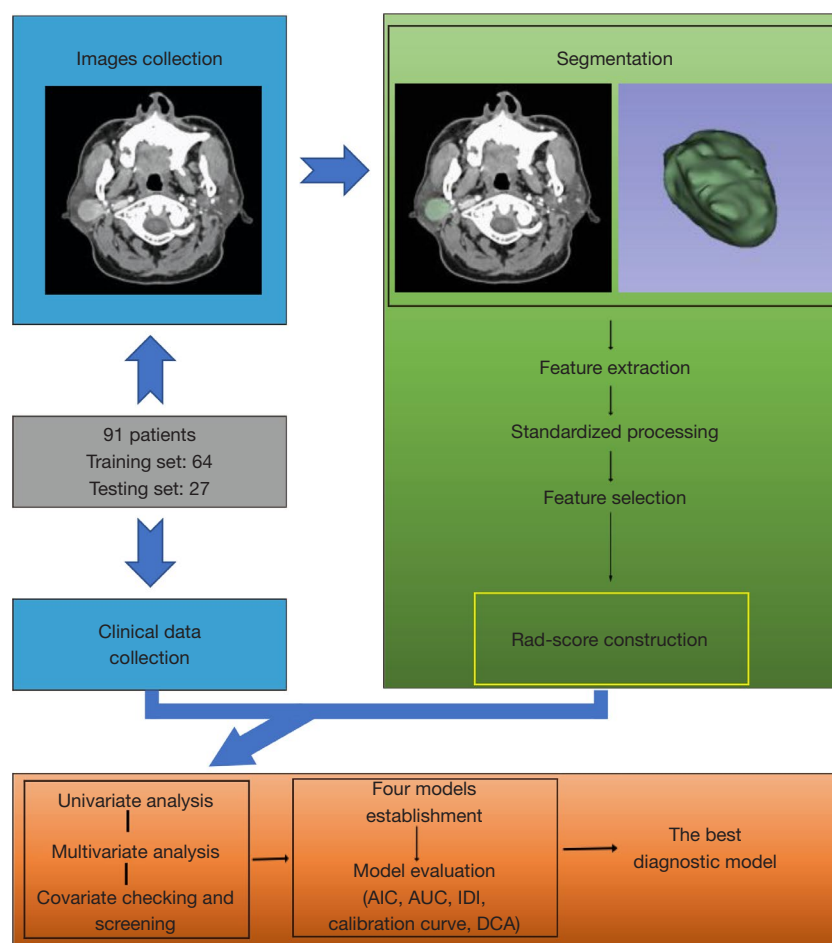


**Figure 1** The flow chart of this study. AIC, Akaike information criterion; AUC, area under the curve; DCA, decision curve analysis; IDI, integrated discrimination improvement index.

is prone to recurrence and has potential for malignant transformation. To date, no published studies have investigated serum AFU levels in patients with PMA and WT, indicating a notable gap in the literature.

The aim of this study was to develop a logistic regression model combining MSCT radiomics and serum AFU to assess the accuracy of distinguishing PMA from WT for assisting in clinic decision-making. We present this study in accordance with the TRIPOD reporting checklist (14) (available at <https://tcr.amegroups.com/article/view/10.21037/tcr-24-871/rc>).

## Methods

Figure 1 illustrates the flow chart of this study.

## Patients

Preoperative enhanced MSCT images, age, gender, and required biochemical indexes [glutamate oxalyl acetate transaminase (AST)/glutamate pyruvate transaminase (ALT), X-protein/globin (X/G), AFU, urea/Cr (U/C), uric acid (UA), high density lipoprotein (HDL), and lactate dehydrogenase (LDH)] were collected from 91 patients with PMA or WT who had parotid tumor resection between December 2017 and December 2021. Exclusion criteria: (I) history of tumor; (II) preoperative radiotherapy or chemotherapy; (III) recurrent parotid tumor; (IV) no surgical treatment or unclear pathological results; and (V) all types of hepatitis.

These patients were randomized into a training cohort and a validation cohort at a ratio of 7:3 (64 vs. 27). The institutional ethics committee of the First Hospital

of Lanzhou University approved this study (No. LDYYLL2022-374). The need for informed consent was waived because of the retrospective nature of the study. This study was conducted in accordance with the Declaration of Helsinki (as revised in 2013).

### *MSCT images acquisition*

All patients underwent a preoperative examination by a dual-source 64-row MSCT scanner (SIEMENS, Erlangen, Germany) with following scanning parameters: tube voltage, 110 kVp; tube current, 130 mAs; matrix, 350×350; gantry rotation time, 0.5 s; pitch, 0.98; collimation, 24 mm × 1.2 mm; scanning slice thickness, 5 mm; reconstruction slice thickness, 1 mm; scanning range, skull base to cervical root. Ioversol was used as the contrast medium with a specification of 50 mL:33.9 g (320 mg iodine per 1 mL), injected through the elbow vein at a rate of 3 mL/s, and the arterial phase images were scanned 30 s after the injection. All images were acquired according to the existing quality control standards and saved in Digital Imaging and Communications in Medicine (DICOM) format.

### *Image segmentation*

Image segmentation includes outlining a lesion from a computed tomography (CT) image, separating it from the surrounding normal tissue, and forming a region of interest (ROI) (15). In this study, two radiologists with more than ten years of experience in head and neck imaging manually outlined the ROI of tumors on each slice of arterial phase images to generate a three-dimensional ROI (Figure 2) using 3D Slicer software (version 4.13; <http://www.slicer.org>). In order to avoid the surrounding normal tissues from being outlined, the two radiologists must draw along the inner 1 mm of the tumor boundary.

### *Feature extraction*

The PyRadiomics software package in Python (version 3.9; <http://www.python.org>) was used to extract radiomics features from each three-dimensional ROI (16). The features were then standardized via Z-score standardization to minimize the influence on the outcomes of subsequent data analysis caused by significant discrepancies in value between features.

### *Inter- and intra-observer reproducible assessment*

To assess intra-observer repeatability, each radiologist followed the same procedure to generate radiomics features twice. Intra-and-inter class correlation (ICC) was used to evaluate the intra- and inter-observer agreement in feature extraction. ICC >0.8 represented good repeatability (17).

### *Feature screening and calculation of Rad-score*

The extracted features with ICC >0.8 in the training cohort were screened using the least absolute shrinkage and selection operator (LASSO) and 5-fold cross-validation. With the addition of penalty parameters to the linear regression model, LASSO, which is based on the least square approach, is used to compress the regression coefficients of variables and some of which may even be compressed to zero. As a consequence, the variables that had a bigger influence on the findings are screened out, and a simpler model is created (18). The regression coefficients are determined by minimizing the following functional equation:

$$J(\beta) = \sum (y - X\beta)^2 + \lambda \|\beta\|_1 = \sum (y - X\beta)^2 + \sum \lambda |\beta| \quad [1]$$

$\lambda \|\beta\|_1$  is the penalty parameter of the objective function,  $\lambda$  is the penalty parameter coefficient, and  $\|\beta\|_1$  is the L1 norm of the regression coefficient  $\beta$ , denoting the sum of the absolute values of all regression coefficients.  $\lambda$  determines the penalty strength of the regression coefficients and controls the goodness-of-fit of the model.  $\lambda$  can be determined by 5-fold cross-validation, and the value of  $\lambda$  that ultimately maximizes the area under the curve (AUC) of the model is the optimal value. The screened features and their corresponding regression coefficients will be obtained once the optimal  $\lambda$  has been determined. Then, the Rad-score for each patient could be calculated by a linear equation consisting of the screened features multiplied by the corresponding regression coefficients.

### *Model establishment*

In the training cohort, the collected variables (AST/ALT, X/G, AFU, U/C, UA, HDL, LDH, gender, and age) and Rad-score were subjected to a univariate logistic regression analysis. Variables with  $P < 0.05$  were then used as confounders, and Rad-score as an exposure variable for covariate checking and screening. The confounders that

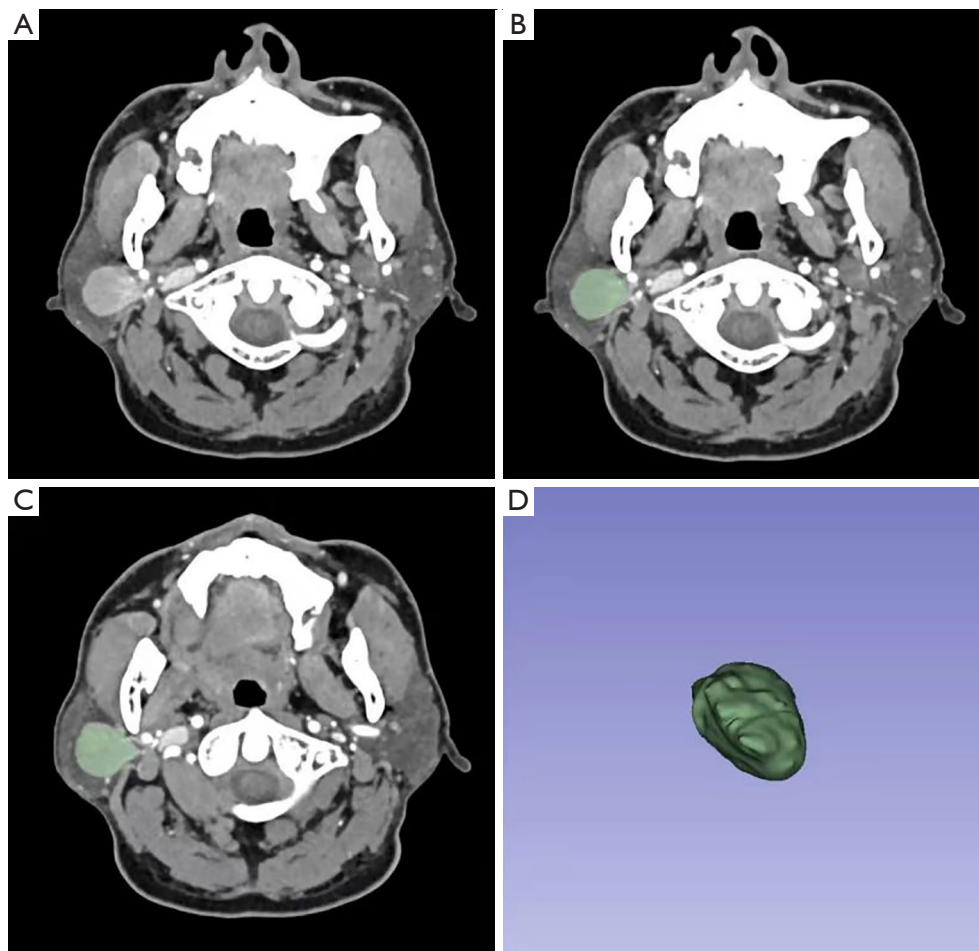


**Figure 2** Outlined diagram of ROI. (A) The MSCT image of the arterial phase shows that there is an abnormal, slightly high-density shadow in the superficial lobe of the right parotid gland, with regular shape and a clear boundary; (B) the ROI of the tumor is manually outlined on the arterial phase image; (C) the ROI of the tumor is manually plotted using the software's auto-identification function; (D) the 3D ROI. ROI, region of interest; MSCT, multi-slice computed tomography; 3D, three-dimensional.

changed the estimate of Rad-score on diagnostic outcomes by more than 10% or were significantly associated with diagnostic outcomes were selected (19). These selected variables were subjected to a multivariate logistic regression analysis along with Rad-score to obtain variables with  $P < 0.05$ . Four diagnostic models were then created using these variables via logistic regression model. As a multivariate analysis method to study the relationship between dichotomous outcomes and some influencing factors, logistic regression model has the objective function as follows (20,21):

$$\text{Logit}(P) = \ln \frac{P}{1-P} = Y = \beta_0 + \beta_1 X_1 + \beta_2 X_2 + \dots + \beta_m X_m \quad [2]$$

$P$  is the probability of the event occurring,  $\beta_0$  is

the intercept,  $\beta_m$  is the regression coefficient of the independent variable  $X_m$ . When  $Y$  varies between  $(-\infty, +\infty)$ ,  $P$  varies between 0 and 1.

#### *Comparison of diagnostic performance and goodness-of-fit*

The validation cohort was used to verify the performance of the four models. The Akaike's information criterion (AIC) as an international standard was used to measure the complexity and goodness-of-fit of the models. The smaller the AIC, the lesser the complexity and the greater the goodness-of-fit (22). To assess the models' diagnostic performance, we compared the receiver operating characteristic (ROC) curve, the AUC, accuracy, sensitivity,



**Table 1** The clinical baseline characteristics of the training and validation cohorts

Clinical factors	Training cohort (n=64)	Validation cohort (n=27)	P value
AST/ALT	1.13 (0.86–1.57)	0.87 (0.71–1.31)	0.02*
X/G	1.70 (1.50–1.90)	1.60 (1.50–1.80)	0.52
AFU (U/L)	18.00 (15.00–22.00)	24.00 (21.00–34.00)	<0.001*
U/C	77.50 (63.00–90.75)	71.00 (62.50–84.00)	0.85
UA (μmol/L)	304.00 (246.00–376.50)	339.00 (263.00–395.00)	0.28
HDL (mmol/L)	1.08 (0.98–1.29)	1.04 (0.94–1.20)	0.30
LDH (U/L)	173.50 (154.75–201.50)	174.00 (162.00–196.00)	0.90
Age (years)	51.00 (40.75–59.00)	51.00 (41.00–56.00)	0.89
Diagnosis			0.76
PMA	47 (73.44)	19 (70.37)	
WT	17 (26.56)	8 (29.63)	
Gender			0.91
Male	34 (53.12)	14 (51.85)	
Female	30 (46.88)	13 (48.15)	

Continuous data are presented as median (interquartile range), while categorical data are presented as counts (percentages). \*,  $P < 0.05$ . AST/ALT, glutamate oxalyl acetate transaminase/glutamate pyruvate transaminase; X/G, X-protein/globin; AFU, alpha-L-fucosidase; U/C, urea/Cr; UA, uric acid; HDL, high density lipoprotein; LDH, lactate dehydrogenase; PMA, pleomorphic adenomas; WT, Warthin tumors.

specificity, positive predictive value, and negative predictive value. The ROC curve was mainly to evaluate the diagnostic performance of dichotomous models. In general, the more convex the curve to the upper left corner, the higher the diagnostic capability. The AUC, whose value ranges from 0.5 to 1, is the area enclosed by the ROC curve and the horizontal and vertical coordinates. Models with AUC values between 0.7 and 0.8 are often considered acceptable, while values between 0.8 and 0.9 indicate moderate diagnostic ability and greater than 0.9 implies excellent diagnostic ability (23). Then, the calibration plot accompanied by Hosmer-Lemeshow test was drawn to evaluate models' goodness-of-fit. Finally, the best model was chosen.

### Evaluation of clinical application value

The decision curve analysis (DCA) was plotted to assess the clinical application value of the best model (24). And the nomogram was drawn for the clinical work.

### Statistical analysis

All statistical analyses were performed by R software (version 3.6.3; <http://www.r-project.org>) (25). Categorical variables

were compared by Chi-square test. Continuous variables were first tested by the Kolmogorov-Smirnov test for conformity to the normal distribution. Student's *t* test, analysis of variance (ANOVA), or Mann-Whitney *U* test was then used for comparison between groups in the corresponding conditions.  $P < 0.05$  was considered to be statistically significant.

## Results

### Patient characteristics

We collected the baseline characteristics (Table 1) of the patients in the training and validation cohorts. The training cohort contained 47 PMA and 17 WT cases. Female number and U/C were significantly higher among PMA cases than in WT cases. Male number, AFU, UA, HDL, LDH, and age were significantly higher among WT cases than in PMA cases ( $P < 0.05$ ).

The validation cohort included 19 PMA cases and 8 WT cases. Similar to the training group, AFU, Age and male number were significantly higher in WT cases. However, different from the training cohort, there was no statistically significant change in U/C, UA, HDL, or LDH between PMA and WT patients. Additionally, in both cohorts, the

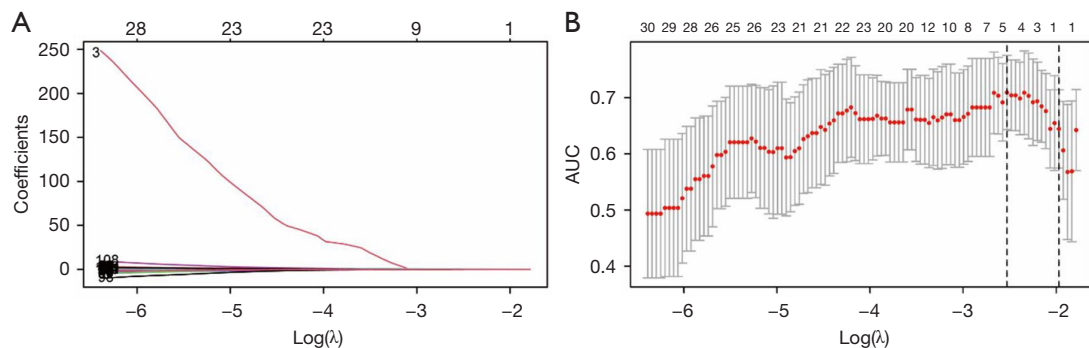


**Figure 3** Screening methods for radiomics features. (A) A curve of the regression coefficients of 112 radiomics features varying with  $\log(\lambda)$ ; (B) the AUC of LASSO regression model varying with  $\log(\lambda)$ . Point A is the  $\log(\lambda)$  value ( $-2.526$ ) when the minimum value ( $\lambda_{\min}=0.080$ ) is taken for  $\lambda$ ; Point B is the  $\log(\lambda)$  value ( $-1.973$ ) when one standard error ( $\lambda_{1se}=0.139$ ) is taken for  $\lambda$ . AUC, the area under the curve; LASSO, least absolute shrinkage and selection operator.

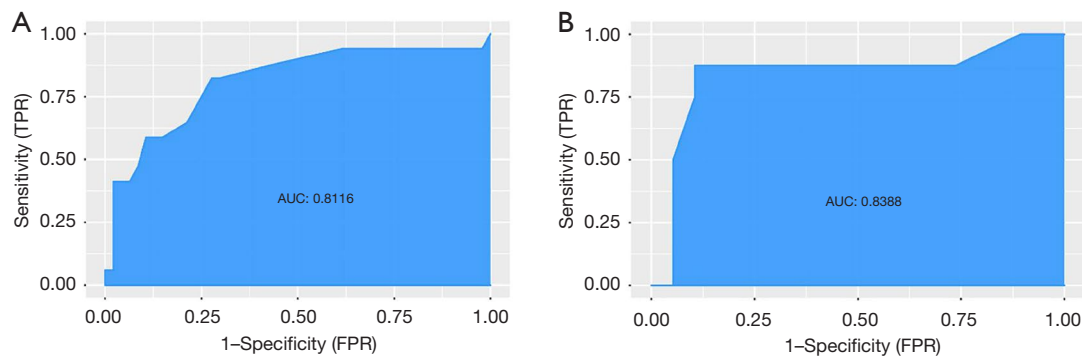


**Figure 4** AUC of LASSO regression model in the training and validation cohorts. (A) AUC of LASSO regression model in the training cohort; (B) AUC of LASSO regression model in the validation cohort. AUC, area under the curve; LASSO, least absolute shrinkage and selection operator; TPR, true positive rate; FPR, false positive rate.

difference in AST/ALT and X/G between PMA and WT was not significant.

#### Feature extraction, screening, and calculation of Rad-score

A total of 112 features with ICC >0.8 were extracted from each three-dimensional ROI, including 19 morphological features (the largest three-dimensional diameter, surface area, volume, shape, voxel number, etc.), 18 grayscale histogram features (skewness, uniformity, mean, median, energy, etc.), and 75 texture features [Grey Level Co-occurrence Matrix (GLCM), Gray Level Size Zone Matrix (GLSZM), Gray Level Run-length Matrix (GLRLM), Neighbourhood Gray-tone Difference Matrix (NGTDM), Grey Level Dependence Matrix (GLDM)] (26).

LASSO regression results show that, as the value of  $\lambda$

increased, the absolute values of the regression coefficients of all features gradually approach 0 and stabilize when  $\lambda$  is around  $-3$  (Figure 3A). 5-fold cross-validation results (Figure 3B) show that when the minimum value (0.080) is taken for  $\lambda$ , the AUC is the largest and 5 features are screened out. The AUCs of the LASSO regression model in the training and validation cohorts are 0.8116 and 0.8388, respectively, indicating that the model has good diagnostic performance (Figure 4). The 5 features and their corresponding regression coefficients are shown in Table 2. The Rad-score for each patient is calculated via the following equation:

$$\begin{aligned} \text{Rad-score} = & -1.083 + 0.104 * \text{Mean} - 0.124 * \text{Flatness} \\ & + 0.076 * \text{Maximum3DDiameter} + 0.417 * \text{Median} \\ & - 0.109 * \text{Large Area Low Gray - Level Emphasis} \end{aligned} \quad [3]$$

Univariate and multivariate logistic regression analysis

Univariate analysis results (Table 3) showed that AFU, U/C, UA, HDL, LDH, Rad-score, gender, and Age were significantly associated with the identification of PMA and WT ( $P<0.05$ ). The odds ratio (OR) revealed that U/C, HDL, and gender were risk factors, AFU, UA, LDH, Rad-score, and age were protective factors. The risk of a parotid tumor being WT increased by 1.05 times for every year of age increase, by 1.15 times for each 1 U/L increase in AFU, by 1.01 times for each 1  $\mu\text{mol/L}$  increase in UA, by 1.02 times for each 1 U/L increase in LDH, and by 12.76 times for each increase in Rad-score. Furthermore, the risk of WT in men was 25 times greater than in women. Covariate checking and screening and multivariate logistic

regression analysis results (Table 3) showed only AFU, Rad-score, and gender were independent diagnostic factors for distinguishing PMA from WT ( $P<0.05$ ).

The establishment of four models

Four diagnostic models were established based on AFU, gender, or Rad-score via logistic regression model (Table 4). The formulas of four models were shown as follows:

Model A1 = 1.67058 + 2.69974 \* Rad-score

Model A2 = 3.10437 + 3.18660 \* Rad-score – 3.84288 \* Gender

Model B1 = 1.82564 + 0.08288 \* AFU – 2.99219 \* Gender

Model B2 = 0.30857 + 0.15995 \* AFU + 3.68124 \* Rad-score – 3.59004 \* Gender

[4]

These formulas also applied to the validation cohort.

Evaluation on diagnostic performance and goodness-of-fit of models

Table 4 shows the AIC of model B2 is the smallest. ROC curves in the training and validation cohorts (Figure 5A, 5B) shows the ROC curve of model B2 is most convex to the upper left corner. Table 5 shows in both cohorts, the AUC sizes of the four models, ranked in descending order, are as follows: model B2 > model A2 > model B1 > model A1. The accuracies of model A2 (0.906) and B2 (0.906) are greater than that of model A1 (0.781) and model B1 (0.781) in the

Table 2 The 5 screened radiomics features and their regression coefficients

Features	Coefficients
Intercept	–1.083
Diagnostics_Image.original_Mean	0.104
Original_shape_Flatness	–0.124
Original_shape_Maximum3DDiameter	0.076
Original_firstorder_Median	0.417
Original_glszm_LargeAreaLowGrayLevelEmphasis	–0.109

Table 3 Univariate and multivariate logistic regression analysis

Variables	Univariate analysis			Multivariate analysis		
	OR	95% CI	P value	OR	95% CI	P value
AST/ALT	0.86	0.27–2.74	0.79		NA	
X/G	1.61	0.17–15.45	0.68		NA	
AFU (U/L)	1.15	1.03–1.28	0.01*	1.18	1.02–1.38	0.03*
U/C	0.96	0.93–0.99	0.01*		NA	
UA ( $\mu\text{mol/L}$ )	1.01	1.00–1.01	0.01*	1.01	1.00–1.01	0.17
HDL (mmol/L)	0.05	0.00–0.90	0.04*		NA	
LDH (U/L)	1.02	1.00–1.04	0.04*		NA	
Rad-score	12.76	3.03–53.81	0.001*	74.34	4.93–1,120.13	0.002*
Gender	0.04	0.00–0.32	0.003*	0.05	0.00–0.88	0.04*
Age	1.05	1.00–1.09	0.03*		NA	

\*,  $P<0.05$ . CI, confidence interval; AST/ALT, glutamate oxalyl acetate transaminase/glutamate pyruvate transaminase; OR, odds ratio; X/G, X-protein/globin; AFU, alpha-L-fucosidase; U/C, urea/Cr; UA, uric acid; HDL, high density lipoprotein; LDH, lactate dehydrogenase; NA, not applicable.



**Table 4** Four models with a combination of AFU, gender or Rad-score

Variables	Model A				Model B			
	Coefficient	95% CI	P value	AIC	Coefficient	95% CI	P value	AIC
Model 1				61.75				59.76
AFU	–	–	–		0.083	0.964–1.224	0.17	
Gender	–	–	–		–2.992	0.006–0.424	0.006*	
Rad-score	2.546	3.424–63.350	<0.001*		–	–	–	
Model 2				46.50				43.33
AFU	–	–	–		0.160	1.016–1.356	0.03*	
Gender	–3.843	0.001–0.176	0.003*		–3.590	0.001–0.273	0.01*	
Rad-score	3.187	3.271–179.151	0.002*		3.681	4.260–369.867	0.001*	

Model A1, (Rad-score); model A2, (Rad-score, gender); model B1, (AFU, gender); model B2, (AFU, Rad-score, gender) (27). \*, P<0.05. AFU, alpha-L-fucosidase; AIC, Akaike's information criterion; CI, confidence interval.

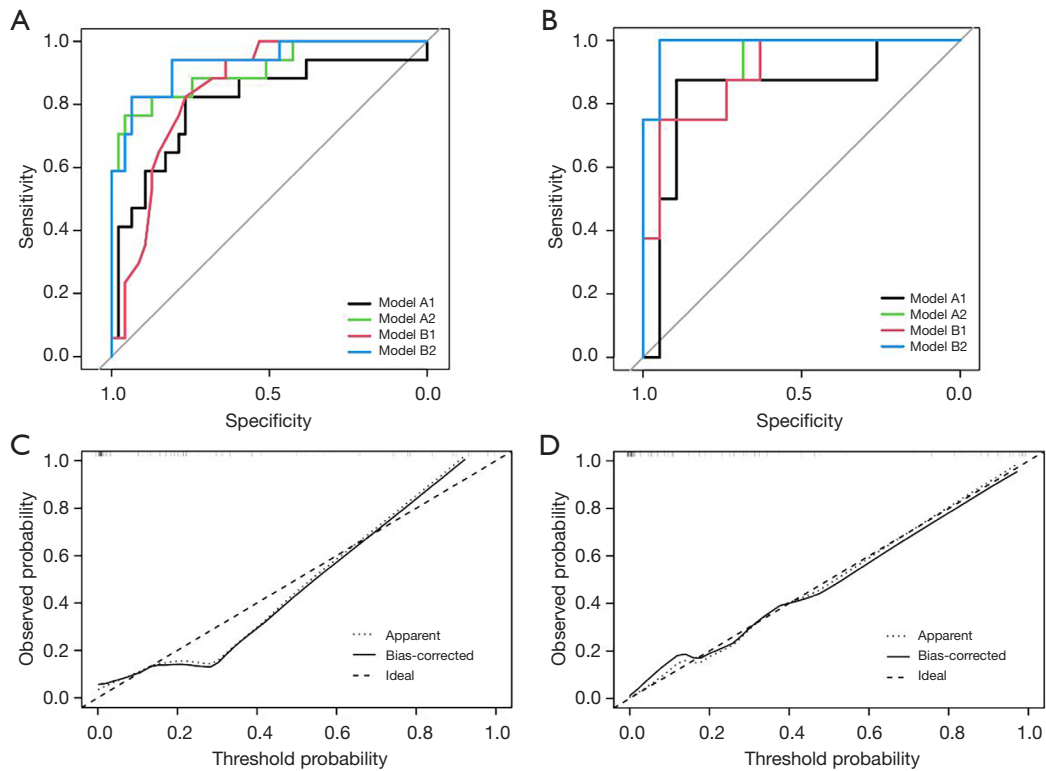


**Figure 5** ROC curves of the four models and calibration curves of model A2 and model B2. (A) ROC curves of the four models in the training cohort; (B) ROC curves of the four models in the validation cohort; (C) calibration curve of model A2 in total patients; (D) calibration curve of model B2 in total patients. Calibration curve shows the consistency between the probability of the tumor predicted as WT and the tumor's actual outcome. The x-axis represents the probability of the tumor predicted as WT and the y-axis represents the tumor's actual outcome. The diagonal dotted line represents a perfect prediction condition of an ideal model (observed probability). The magenta line represents the performance of the two models (model A2 and model B2). The closer the data points are to the diagonal dotted line, the better the predictive effect of the model. Model A1, (Rad-score); model A2, (Rad-score, gender); model B1, (AFU, gender); model B2, (AFU, Rad-score, gender) (27). ROC, receiver operating characteristic; WT, Warthin tumors; AFU, alpha-L-fucosidase.

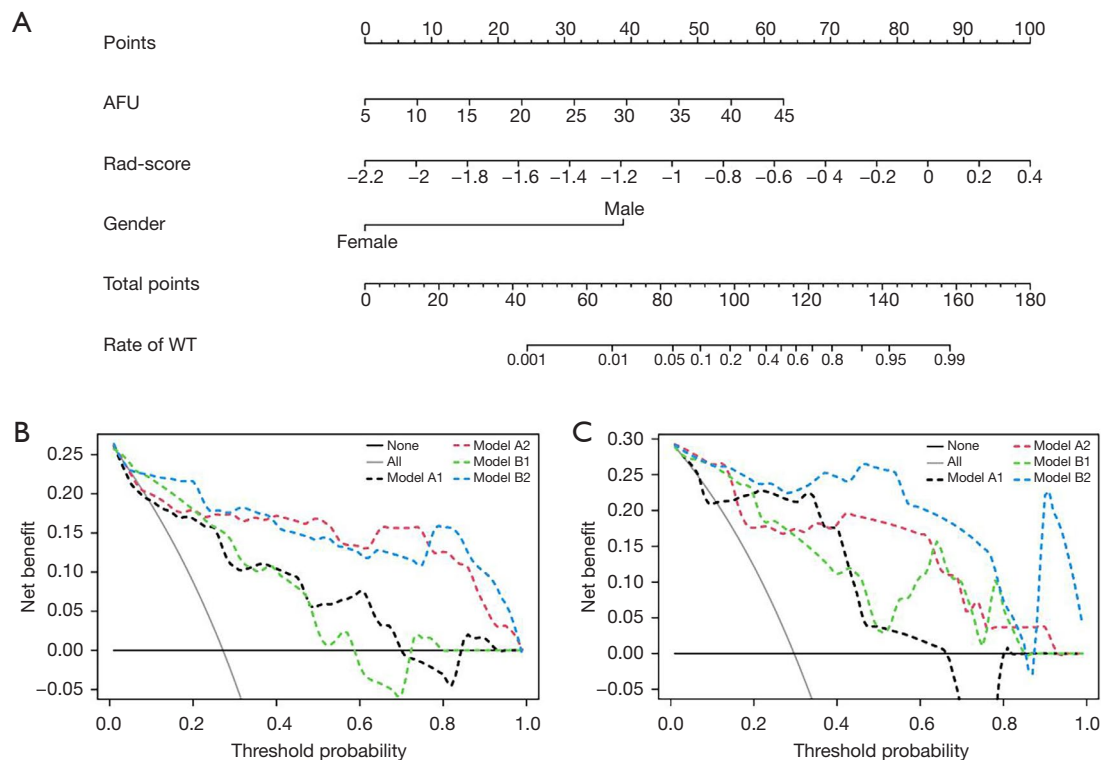


**Figure 6** Nomogram of model B2 and DCA curves of the four models. (A) Nomogram of model B2. The values of each of the three variables are plotted as vertical lines toward the Points axis to determine the corresponding points, the sum of the three points corresponded to the Total Points axis, and plotted as vertical lines toward the rate of WT axis, and the corresponding value is the probability that the parotid tumor being WT. The tumor could be diagnosed as WT if the rate of WT >0.595. (B) DCA curves of the four models in the training cohort; (C) DCA curves of the four models in the validation cohort. The abscissa represents the threshold probability, and the ordinate represented the net benefit. The horizontal line indicates that all patients are diagnosed with PMA and treated with PSP or SP, with the net benefit of 0; the slash line indicates that all patients are diagnosed with WT and treated with extracapsular dissection, and the net benefit is a backslash with a negative slope. The remaining four curves represented the four models (see legend for identification), respectively. It shows that within a large range of threshold probability, the net benefit of model B2 is higher than the other three models. Model A1, (Rad-score); model A2, (Rad-score, gender); model B1, (AFU, gender); model B2, (AFU, Rad-score, gender) (27). DCA, decision curve analysis; AFU, alpha-L-fucosidase; WT, Warthin tumors; PSP, partial superficial parotidectomy; SP, superficial parotidectomy.

training cohort. In the validation cohort, the accuracies of model A1, A2, and B1 are all 0.889, which are lower than that of model B2 (0.963), indicating that model A2 and B2 had higher diagnostic performance than the other two models, and model B2 had the greatest. The calibration plots of model A2 and B2 (Figure 5C,5D) shows that the calibration curve of model B2 is closer to the diagonal dotted line, indicating the predicting effect of model B2 is better than that of model A2. Hosmer-Lemeshow test shows model B2 ( $\chi^2=0.055$ ,  $df=2$ ,  $P=0.75$ ) has better goodness-of-fit than that of model A2 ( $\chi^2=4.123$ ,  $df=2$ ,  $P=0.12$ ). Thus, model B2 performs best among the four models.

### Evaluation of clinical value of model B2

The nomogram of model B2 is illustrated in Figure 6A. The best threshold of the nomogram in the training cohort was 0.385 (Table 5), then the best probability value P was calculated via Eq. [5]:

$$P = \frac{e^Y}{1 + e^Y} = \frac{e^{0.385}}{1 + e^{0.385}} = 0.595 \quad [5]$$

As a result, when the rate of WT calculated by the nomogram was greater than 0.595, the tumor could be diagnosed as WT.

The DCA curves of four models in the training and

**Table 5** AUC and accuracy of four models in the training and validation cohorts

Model	AUC (95% CI)	Specificity	Sensitivity	Best threshold	Accuracy	Positive-pv	Negative-pv
Training cohort							
A1	0.807 (0.670–0.945)	0.766	0.824	–0.988	0.781	0.560	0.923
A2	0.910 (0.820–1.000)	0.957	0.765	–3.861	0.906	0.867	0.918
B1	0.848 (0.754–0.942)	0.766	0.824	–3.450	0.781	0.560	0.923
B2	0.934 (0.863–1.000)	0.936	0.824	–4.060	0.906	0.824	0.936
Validation cohort							
A1	0.842 (0.649–1.000)	0.895	0.875	–0.578	0.889	0.778	0.944
A2	0.908 (0.794–1.000)	0.947	0.750	–3.764	0.889	0.857	0.900
B1	0.901 (0.780–1.000)	0.947	0.750	–2.414	0.889	0.857	0.900
B2	0.987 (0.956–1.000)	0.947	1.000	–3.587	0.963	0.889	1.000

Model A1, (Rad-score); model A2, (Rad-score, gender); model B1, (AFU, gender); model B2, (AFU, Rad-score, gender) (27). AUC, area under the curve; CI, confidence interval; Positive-pv, positive predict value; Negative-pv, negative predict value.

validation cohorts (*Figure 6B,6C*) shows that within the threshold probability (10–60%), all models are available, and the net benefit of model B2 was greater than that of the others in the validation cohort, indicating that model B2 had the highest clinical application value.

Discussion

The most common benign tumors of parotid glands are PMA and WT (28), the former is more prone to malignant transformation and recurrence than the latter, resulting in significant differences in surgical therapies (1). Therefore, accurate differentiation of PMA from WT is vital for the prognosis of patient. Ultrasound, as the preferred method of body surface imaging, plays an important role in the differential diagnosis of parotid masses. However, ultrasound requires the operators to have possess a high level of examination skills and it is difficult to assess the nature of lesions in deeper sites. In addition to ultrasound, other imaging examinations such as CT and magnetic resonance imaging (MRI) are also widely used in the preoperative diagnosis of parotid tumors. Among different examination methods, CT is minimally invasive, affordable, low-risk, and can locate the three-dimensional position of the mass and analyze the relationship between the mass and the surrounding tissues, which is becoming the main choice for preoperative examination of parotid tumors in China (29). CT has been proven to have a high degree of accuracy in identifying parotid tumors, but the majority

of this evidence has relied on the visual assessment of qualitative or semi-quantitative features such as tumor morphology, border, location, diameter, and density values in the images, which is a highly subjective approach that may lead to misdiagnosis (2). In contrast, the diagnostic model we developed is based on objective variables such as serum AFU, gender, and Rad-score. In this retrospective study, we developed and validated a MSCT-based radiomics model that integrates AFU and gender for the differentiation of PMA from WT. The presented radiomics model showed powerful discrimination efficacy in both the training cohort (AUC 0.934) and the validation cohort (AUC 0.987).

Clinically, we found a significant difference in the values of some blood examination indices, especially AFU, between PMA and WT patients. Serum AFU is a common blood examination index that is currently used to assess liver function. Previous research has shown that serum AFU levels were significantly associated with favorable progression-free survival in breast cancer patients treated with trastuzumab, and therefore serum AFU may be considered as a biomarker for predicting trastuzumab sensitivity (30). In addition, serum AFU levels were found to be significantly different in patients with oral precancerous lesions and oral cancer compared to normal subjects, suggesting that serum AFU could be used as a biomarker for early oral cancer screening and tracking therapy effectiveness (31). However, studies on serum AFU levels in patients with parotid tumors have

not been reported. Therefore, in this study, we analyzed these blood examination indices (*Table 1*) by univariate and multivariate logistic regression analysis, and the results showed that only AFU was an independent diagnostic factor in the differentiation between PMA and WT. We found that patients with PMA had lower serum AFU levels than patients with WT, and the difference was statistically significant (*Table 3*). Considering that PMA has the property of being susceptible to malignant transformation and recurrence, we believe that serum AFU levels can be used as a biomarker to predict the probability of recurrence or malignant transformation in PMA (32).

Radiomics is a hotspot of current research as an emerging technology (33). In about 10 years since it was initially presented in 2012, radiomics has been demonstrated to be useful for the prediction of preoperative lymph node metastasis and vascular infiltration in cancer patients (34), as well as the prognosis of cancer and cerebral hemorrhage patients (35). In this study, we screened 112 extracted radiomics features, but only 5 of them—3 morphological features and 2 textural features—were ultimately connected to the differentiation of PMA and WT. The remaining features were redundant or unrelated, which is consistent with the findings of previous studies. The large difference in textural features between PMA and WT may be due to the fact that the former is mainly composed of glandular duct-like, mucus-like, or cartilaginous tissue, whereas the latter is mainly composed of glandular epithelial and lymphatic tissue, and the latter has a slightly higher probability of cystic degeneration.

Herein, we developed and validated a prediction model based on AFU, gender and Rad-score for differentiating PMA and WT. The diagnostic performance of this model was superior to the remaining three models both in the training and validating cohorts. Therefore, the nomogram based on the best model in this study can be used as an auxiliary tool for clinicians to differentiate PMA and WT preoperatively.

There are some limitations in this study that should be acknowledged. First, it was possible that this study had sampling bias. In the process of collecting patient data, we excluded more cases, such as recurrent tumors, cases without preoperative MSCT-enhanced scans, cases in which the MSCT images were so unclear that the tumor borders could not be identified, etc. Second, this study was a single-center one with a relatively small sample size. In the future, we will continue to collect relevant data to validate the clinical value of the diagnostic model developed in this study.

Third, this study lacks external validation, which limits the generalizability of the diagnostic model to other clinical settings. Future studies will aim to validate this model with external datasets from multiple centers to ensure its robustness and applicability across different populations.

## Conclusions

In conclusion, we found that preoperative serum AFU levels could be used as a useful biomarker to differentiate PMA from WT. We further developed and validated a nomogram based on Rad-score, gender and serum AFU, which was proved to be highly accurate in distinguishing PMA from WT. This work could give clinicians fresh perspectives and techniques for figuring out the kind of parotid tumors before surgery.

## Acknowledgments

We thank all of those who helped us with this retrospective study.

*Funding:* This work was supported by grants from the National Natural Science Foundation of China (No. 82260477).

## Footnote

*Reporting Checklist:* The authors have completed the TRIPOD reporting checklist. Available at <https://tcr.amegroups.com/article/view/10.21037/tcr-24-871/rc>

*Data Sharing Statement:* Available at <https://tcr.amegroups.com/article/view/10.21037/tcr-24-871/dss>

*Peer Review File:* Available at <https://tcr.amegroups.com/article/view/10.21037/tcr-24-871/prf>

*Conflicts of Interest:* All authors have completed the ICMJE uniform disclosure form (available at <https://tcr.amegroups.com/article/view/10.21037/tcr-24-871/coif>). The authors have no conflicts of interest to declare.

*Ethical Statement:* The authors are accountable for all aspects of the work in ensuring that questions related to the accuracy or integrity of any part of the work are appropriately investigated and resolved. The institutional ethics committee of the First Hospital of Lanzhou University approved this study (No. LDYYLL2022-374).

This study was conducted in accordance with the Declaration of Helsinki (as revised in 2013). The need for informed consent was waived because of the retrospective nature of the study.

**Open Access Statement:** This is an Open Access article distributed in accordance with the Creative Commons Attribution-NonCommercial-NoDerivs 4.0 International License (CC BY-NC-ND 4.0), which permits the non-commercial replication and distribution of the article with the strict proviso that no changes or edits are made and the original work is properly cited (including links to both the formal publication through the relevant DOI and the license). See: <https://creativecommons.org/licenses/by-nc-nd/4.0/>.

## References

- Zheng YM, Chen J, Xu Q, et al. Development and validation of an MRI-based radiomics nomogram for distinguishing Warthin's tumour from pleomorphic adenomas of the parotid gland. *Dentomaxillofac Radiol* 2021;50:20210023.
- Zhang D, Li X, Lv L, et al. Improving the diagnosis of common parotid tumors via the combination of CT image biomarkers and clinical parameters. *BMC Med Imaging* 2020;20:38.
- Hou Z, Li S, Jiang Y, et al. Benefits of intraoral stents for sparing normal tissue in radiotherapy of nasopharyngeal carcinoma: a radiobiological model-based quantitative analysis. *Transl Cancer Res* 2021;10:4281-9.
- Li ZQ, Gao JN, Xu S, et al. Multimodal magnetic resonance imaging for the diagnosis of parotid gland malignancies: systematic review and meta-analysis. *Transl Cancer Res* 2022;11:2275-82.
- Cheng PC, Chang CM, Huang CC, et al. The diagnostic performance of ultrasonography and computerized tomography in differentiating superficial from deep lobe parotid tumours. *Clin Otolaryngol* 2019;44:286-92.
- Mayerhoefer ME, Materka A, Langs G, et al. Introduction to Radiomics. *J Nucl Med* 2020;61:488-95.
- Lambin P, Rios-Velazquez E, Leijenaar R, et al. Radiomics: extracting more information from medical images using advanced feature analysis. *Eur J Cancer* 2012;48:441-6.
- Avanzo M, Stancanella J, Pirrone G, et al. Radiomics and deep learning in lung cancer. *Strahlenther Onkol* 2020;196:879-87.
- Hu Y, Tang D, Zhang P. Prognostic and immunological role of alpha-L-fucosidase 2 (FUCA2) in hepatocellular carcinoma. *Transl Cancer Res* 2023;12:257-72.
- Deugnier Y, Le Treut A, Glaire D, et al. A study of lysosomal enzyme activities in serum and leukocytes in chronic hepatic disease (author's transl). *Clin Chim Acta* 1980;108:385-92.
- Ezawa I, Sawai Y, Kawase T, et al. Novel p53 target gene FUCA1 encodes a fucosidase and regulates growth and survival of cancer cells. *Cancer Sci* 2016;107:734-45.
- Otero-Estévez O, Martínez-Fernández M, Vázquez-Iglesias L, et al. Decreased expression of alpha-L-fucosidase gene FUCA1 in human colorectal tumors. *Int J Mol Sci* 2013;14:16986-98.
- Shah M, Telang S, Raval G, et al. Serum fucosylation changes in oral cancer and oral precancerous conditions: alpha-L-fucosidase as a marker. *Cancer* 2008;113:336-46.
- Moons KG, Altman DG, Reitsma JB, et al. New Guideline for the Reporting of Studies Developing, Validating, or Updating a Multivariable Clinical Prediction Model: The TRIPOD Statement. *Adv Anat Pathol* 2015;22:303-5.
- Sun L, Fu Y, Zhao J, et al. MAS-CL: An End-to-End Multi-Atlas Supervised Contrastive Learning Framework for Brain ROI Segmentation. *IEEE Trans Image Process* 2024;33:4319-33.
- Wang T, She Y, Yang Y, et al. Radiomics for Survival Risk Stratification of Clinical and Pathologic Stage IA Pure-Solid Non-Small Cell Lung Cancer. *Radiology* 2022;302:425-34.
- Shrout PE, Fleiss JL. Intraclass correlations: uses in assessing rater reliability. *Psychol Bull* 1979;86:420-8.
- Trayanova NA, Popescu DM, Shade JK. Machine Learning in Arrhythmia and Electrophysiology. *Circ Res* 2021;128:544-66.
- Jaddoe VW, de Jonge LL, Hofman A, et al. First trimester fetal growth restriction and cardiovascular risk factors in school age children: population based cohort study. *BMJ* 2014;348:g14.
- Meurer WJ, Tolles J. Logistic Regression Diagnostics: Understanding How Well a Model Predicts Outcomes. *JAMA* 2017;317:1068-9.
- Liu P, Xing Z, Peng X, et al. Machine learning versus multivariate logistic regression for predicting severe COVID-19 in hospitalized children with Omicron variant infection. *J Med Virol* 2024;96:e29447.
- Portet S. A primer on model selection using the Akaike Information Criterion. *Infect Dis Model* 2020;5:111-28.
- Messina A, Chew M, Cecconi M. Rotten and gold apples: inside and outside the gray zone of a ROC curve. *Crit Care* 2024;28:22.



24. Adamson AS, Abraham I. Decision Curve Analysis and the Net Benefit of Novel Tests. *JAMA Dermatol* 2022;158:684.
25. Zhang D, Zhu W, Guo J, et al. Application of artificial intelligence in glioma researches: A bibliometric analysis. *Front Oncol* 2022;12:978427.
26. Demircioglu A. Radiomics-AI-based image analysis. *Pathologie* 2019;40:271-6.
27. Kushima M, Kojima R, Shinohara R, et al. Association Between Screen Time Exposure in Children at 1 Year of Age and Autism Spectrum Disorder at 3 Years of Age: The Japan Environment and Children's Study. *JAMA Pediatr* 2022;176:384-91.
28. Liu Y, Zheng J, Lu X, et al. Radiomics-based comparison of MRI and CT for differentiating pleomorphic adenomas and Warthin tumors of the parotid gland: a retrospective study. *Oral Surg Oral Med Oral Pathol Oral Radiol* 2021;131:591-9.
29. Li Q, Jiang T, Zhang C, et al. A nomogram based on clinical information, conventional ultrasound and radiomics improves prediction of malignant parotid gland lesions. *Cancer Lett* 2022;527:107-14.
30. Matsumoto K, Shimizu C, Arai T, et al. Identification of predictive biomarkers for response to trastuzumab using plasma FUCA activity and N-glycan identified by MALDI-TOF-MS. *J Proteome Res* 2009;8:457-62.
31. Vajaria BN, Patel KA, Patel PS. Role of aberrant glycosylation enzymes in oral cancer progression. *J Carcinog* 2018;17:5.
32. Levyn H, Subramanian T, Eagan A, et al. Risk of Carcinoma in Pleomorphic Adenomas of the Parotid. *JAMA Otolaryngol Head Neck Surg* 2023;149:1034-41.
33. Sunnetci KM, Kaba E, Celiker FB, et al. Deep Network-Based Comprehensive Parotid Gland Tumor Detection. *Acad Radiol* 2024;31:157-67.
34. Chen J, He B, Dong D, et al. Noninvasive CT radiomic model for preoperative prediction of lymph node metastasis in early cervical carcinoma. *Br J Radiol* 2020;93:20190558.
35. Mayerhoefer ME, Riedl CC, Kumar A, et al. Radiomic features of glucose metabolism enable prediction of outcome in mantle cell lymphoma. *Eur J Nucl Med Mol Imaging* 2019;46:2760-9.

**Cite this article as:** Yan Q, Liao L, Wang X, Zeng X, Zhang L, He D. Multi-slice computed tomography radiomics combined with serum alpha-L-fucosidase: a potential biomarker for precise identification of pleomorphic adenoma and Warthin tumor. *Transl Cancer Res* 2024;13(12):6793-6806. doi: 10.21037/tcr-24-871